JOURNAL OF MODERN OPTICS, 1998, VOL. 45, NO. 6, 1099–1110

Nonlinear competing processes in multifrequency Raman generation

G. S. McDONALD, G. H. C. NEW, YUK-MING CHAN

Laser Optics and Spectroscopy Group, The Blackett Laboratory, Imperial College of Science, Technology and Medicine, Prince Consort Road, London SWT 2BZ.

L. L. LOSEV and A. P. LUTSENKO

P. N. Lebedev Physical Institute, Leninsky Prospekt 53, 117924 Moscow.

(*Received 15 September 1997*)

Abstract. We investigate the extent to which the Raman generation of ultrabroad-band light will be affected by nonlinear competing processes. The model equations are generalized to incorporate an off-axis competing signal and a quantitative study is undertaken of its affect on the primary process. An effective gain–length product for the parasitic process is introduced and its characteristics examined. A simple analytical model has been developed for the case of a competing process generated from background noise or amplified spontaneous emission. Predictions of this model are found to be in good agreement with numerical simulations. We find that the efficiency and character of ultrabroad-band multifrequency Raman generation, with resonant and symmetric pumping, effectively drives such nonlinear competing processes below threshold. The roles played by dispersion, transiency and the initial intensity of the competing process are all systematically investigated. Multi-frequency conversion is also found to be robust when the competing signal grows from a strong seed, as could arise from scattering of a pump beam.

1. Introduction

Ultrabroad-band multifrequency Raman generation (UMRG) is one of the most novel nonlinear optical processes to have emerged over the last few years. With H_2 gas as the Raman medium, our analyses have predicted that nearly 50 distinct frequencies of comparable energy may be generated [1–4]. More recent calculations for UMRG in air at atmospheric pressure have predicted that beams containing around 150 waves may be attained [5]. The richness of the subject leads to connections with a large number of distinct research areas, reflecting the unusual breadth of potential applications (which include frequency conversion, atmospheric transmission of optical energy and information, sensing, visual displays, measurement techniques, spectroscopy and inertial confinement fusion).

In conventional stimulated Raman scattering, all or nearly all the input optical energy is delivered in the form of a single beam at the pump frequency. This results in the excitation of many competing rotational and vibrational transitions,

0950–0340/98 $12·00

each with its own Stokes shift [6]. For relatively long input pulses, and only a single Raman process, the efficiency of energy conversion to the Stokes frequency is determined, to a large extent, by a gain–length product $Z = gI_0z$, where g is the steady-state gain coefficient for the transition, I_0 is the (undepleted) pump intensity and z is the interaction distance. For typical levels of spontaneous emission at the Stokes frequency and background loss, one can define a threshold $Z^{\text{th}} \approx 25$, for which 1% conversion of the pump energy is obtained [7]. By contrast, UMRG is initiated by *resonant symmetric pumping*, in which the incident energy is divided equally between two (linearly polarized) collinear beams, their frequency difference being matched to the rotational Raman transition which has the highest gain [1–5]. Through a combination of parametric and non-parametric processes, this leads to a very rapid and even redistribution of the input energy to both (lower-frequency) Stokes and (higher-frequency) anti-Stokes components. The resulting spectrum forms a uniform comb in frequency space with an overall bandwidth that can approach the pump carrier frequency. The UMRG process starts for values of Z as low as 0.1.

Experimental results, that support our overall predictions of UMRG using H_2 gas, are appearing in the literature [8–12]. However, results to date have demonstrated that competition may exist between several different Raman resonances. In this case, frequency components in the output spectra are not uniformly spaced. We note that many of the proposed applications of UMRG benefit greatly from (or even rely upon) a uniform frequency comb. Furthermore, it is likely that such competition reduces the efficiency of the dominant UMRG process and leads to an output bandwidth less than the theoretical maximum. The objective of this paper is to quantify the role that competing nonlinear processes play in UMRG when a single rotational transition of H_2 gas is resonantly driven. It is of central importance to determine whether parasitic processes are avoidable in UMRG and whether their occurrence in experiments is simply the result of a choice of system parameters. To address this question, we have generalized our model equations to include a competing Raman process and have undertaken a quantitative study to explore whether or not such additional processes are inherent to UMRG.

2. Model equations

We begin with a brief overview of the UMRG equations which we shall subsequently generalize to include a competing process. The electric field is expanded in plane waves whose frequencies are given by $\omega_n = \omega_0 + n\omega_{\text{R}}$ where $n = 0, \pm1, \pm2, \ldots$ and ω_0 and ω_{R} are the pump frequency and Stokes shift respectively. One obtains the following dimensionless equations for the complex field amplitudes A_n and the associated polarization wave amplitude P [1, 2, 13]:

$$\frac{\partial A_n}{\partial Z} = \frac{\omega_n}{2\omega_0}[P^* A_{n+1} \exp(-\mathrm{i}\gamma_{n+1}Z) - PA_{n-1} \exp(\mathrm{i}\gamma_n Z)], \tag{1}$$

$$\frac{T_2}{t_{\text{p}}}\frac{\partial P}{\partial \tau} = -P + \sum_j A_j A_{j-1}^* \exp(-\mathrm{i}\gamma_j Z). \tag{2}$$

The fields A_n are normalized to the peak input amplitude at the pump frequency, so that the maximum value of $|A_0(Z=0)|$ is unity; $Z = gI_0z$ is the steady-state

gain–length product and can be considered as a normalized propagation distance in the context of the model; τ is local time (in units of input pulse width t_p) and T_2 is the medium dephasing time. Dispersion gives rise to a set of normalized mismatch parameters $\gamma_n = [(\Delta k_n - \Delta k_{n-1}) - (\Delta k_0 - \Delta k_{-1})]/gI_0$, where $\Delta k_n = (\mu_n - 1)\omega_n/c$ and μ_n is the refractive index at ω_n. Assuming a Cauchy formula for the frequency dependence of μ_n, one finds that $\gamma_n = n\gamma_1[1 + (n-1)\omega_R/2\omega_0]$. Thus, for any particular choice of ω_R/ω_0, γ_1 determines the full set of γ_n values. We consider symmetric pumping with Gaussian pulses, $A_0(\tau) = A_{-1}(\tau) = \exp(-\tau^2)$ at $Z = 0$, and assume that this pumping is exactly tuned to a Raman resonance. Nearly all the experimental work published to date has dealt with UMRG in H_2 gas. For H_2 at 1 atm, the highest gain coefficient corresponds to the S(1) rotational transition, for which $g = 0.2\,\mathrm{cm\,GW^{-1}}$. We consider pump beams which are supplied by the second harmonic of a Nd-doped yttrium aluminium garnet laser and a Raman sideband, giving $\omega_0/2\pi c = 18\,900\,\mathrm{cm^{-1}}$ and $\omega_R/2\pi c = 587\,\mathrm{cm^{-1}}$.

To undertake a rigorous examination of the role of competing processes, one would need to consider a large number of distinct Raman transitions. Moreover, the Raman sidebands associated with each of these transitions would need to be included in the model equations. However, for UMRG in H_2 with only a *single* Raman transition, around 100 complex field envelopes are involved. To simulate the interaction of waves arising from many distinct transitions would therefore require enormous computational resources. We therefore consider a *worst-case* scenario in which there is only one competing process which does not have to share the pump energy with any others. To maximize the gain available to the competing process, we shall consider the amplification of a signal A'_{-1} at the Stokes frequency ω_{-1}. For the propagation of this parasitic wave at an angle θ'_{-1} to the multi-frequency beam [13], the polarization wave is decomposed into two parts: $P \to P + P' \exp(-i\Delta'_0 z)$ where $\Delta'_0 = \Delta k_{-1} - \Delta k'_{-1} = \mu_{-1}\omega_{-1}(1 - \cos\theta'_{-1})/c$. The UMRG model equations then become

$$(\text{for } n \neq 0)\quad \frac{\partial A_n}{\partial Z} = \frac{\omega_n}{2\omega_0}[P^* A_{n+1} \exp(-i\gamma_{n+1} Z) - P A_{n-1} \exp(i\gamma_n Z)], \tag{3}$$

$$\frac{\partial A_0}{\partial Z} = \tfrac{1}{2}[P^* A_1 \exp(-i\gamma_1 Z) - P A_{-1} \exp(i\gamma_0 Z) - P' A'_{-1}], \tag{4}$$

$$\frac{\partial A'_{-1}}{\partial Z} = \frac{\omega_{-1}}{2\omega_0} P'^* A_0, \tag{5}$$

$$\frac{T_2}{t_p}\frac{\partial P}{\partial \tau} = -P + \sum_j A_j A^*_{j-1} \exp(-i\gamma_j Z), \tag{6}$$

$$\frac{T_2}{t_p}\frac{\partial P'}{\partial \tau} = -P' + A_0 A'^*_{-1}. \tag{7}$$

Comparing systems (1)–(2) and (3)–(7), it can be seen that the UMRG equations are supplemented with the additional (off-axis) polarization wave P' which is driven by the grating formed by the interaction of the parasitic process and the pump wave A_0. In the numerical simulation of equations (3)–(7), we shall assume that the normalized interaction length for the competing process is equal to that of the main UMRG process. This is a rather pessimistic assumption since finite

θ'_{-1} gives rise to a progressive reduction in the overlap integral of the two processes.

3. Steady-state ultrabroad-band multifrequency Raman generation

In this section, we investigate UMRG with continuous-wave (CW) beams (steady-state interactions). Since the components of the polarization wave follow their source terms adiabatically in this limit, the full set of generalized multi-frequency equations can be simplified. Setting $\partial P/\partial\tau = \partial P'/\partial\tau = 0$ in equations (6) and (7), so that $P(\tau) \to P_{ss}$ and $P'(\tau) \to P'_{ss}$, one finds that

$$(\text{for } n \neq 0)\ \frac{\partial A_n}{\partial Z} = \frac{\omega_n}{2\omega_0}[P^*_{ss}A_{n+1}\exp(-i\gamma_{n+1}Z) - P_{ss}A_{n-1}\exp(i\gamma_n Z)], \tag{8}$$

$$\frac{\partial A_0}{\partial Z} = \tfrac{1}{2}[P^*_{ss}A_1\exp(-i\gamma_1 Z) - P_{ss}A_{-1}\exp(i\gamma_0 Z) - |A'_{-1}|^2 A_0], \tag{9}$$

$$\frac{\partial A'_{-1}}{\partial Z} = \frac{\omega_{-1}}{2\omega_0}|A_0|^2 A'_{-1}, \tag{10}$$

$$P_{ss} = \sum_j A_j A^*_{j-1}\exp(-i\gamma_j Z). \tag{11}$$

In the steady-state model, the coupling of UMRG and the competing process, via P'_{ss}, reduces to two (automatically phase-mached) intensity-dependent terms. Consequently, P'_{ss} does not appear explicitly in the above equations.

3.1. *Spontaneous generation and amplified spontaneous emission*

We first consider the generation of a competing process from background noise or amplified spontaneous emission (ASE). The initial intensity of the parasitic wave will then be very small ($|A'_{-1}(0)|^2 = 10^{-m}$, where $m > 10$) and any significant conversion of pump energy to the competing wave will typically require a gain–length product of around 25 [7]. It is obvious that the initial stages of UMRG will be unaffected by the amplification of such a low-intensity seed. As a prelude to our study, we begin by looking at the properties of UMRG when the additional process is absent.

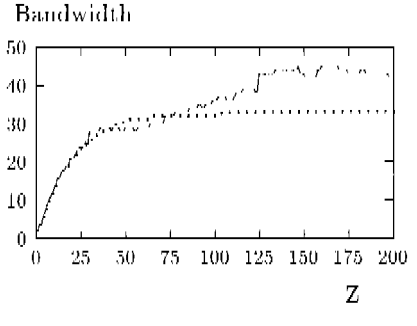

Figure 1. Evolution of the bandwidth of a multifrequency beam propagating through a 2 m cell of H_2 gas at a pressure of 1 atm, where the dimensionless parameter Z can be interpreted as a distance (in centimetres): (· · · · ·), the solution when background dispersion is neglected; (——) the bandwidth growth when dispersion is accounted for.

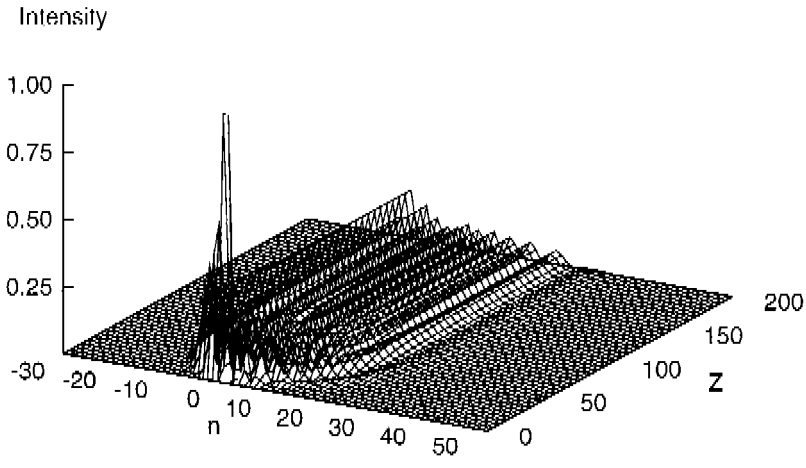

(*a*)

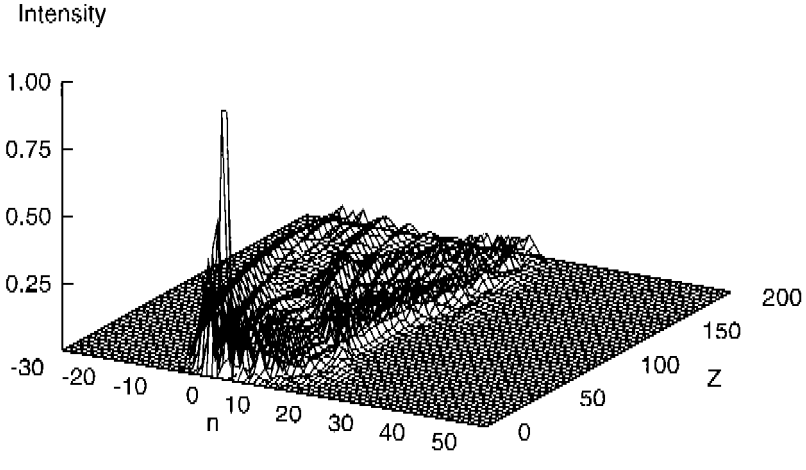

(*b*)

Figure 2. Growth of the spectrum of the multifrequency beam with normalized distance Z, where individual frequency channels are labelled using the index n: (*a*) dispersionless solution; (*b*) the solution when background dispersion is included.

If we set $gI_0 = 1\,\mathrm{cm}^{-1}$, the normalized distance Z can be interpreted as a length in centimeters. Then, for H_2 gas at 1 atm, one finds that $\gamma_1 \approx 2.5 \times 10^{-3}$ [2]. Figure 1 shows the bandwidth of the multifrequency beam, defined as the number of frequency components of comparable intensity, as a function of Z for $\gamma_1 = 0$ (the dispersionless case) and $\gamma_1 = 2.5 \times 10^{-3}$. In the former case, the bandwidth saturates at a level given by $B = B_0 = \omega_0/\omega_R \approx 32$ [1] whereas, when dispersion is included, the bandwidth continues to grow along the cell [2]. The development of the spectrum for each case is shown in figure 2. In the dispersionless case, the UMRG spectrum converges to a fixed pattern since the polarization wave becomes exhausted ($P \to 0$) through multifrequency gain suppression [2, 5]. The role of dispersion is to offset gain suppression. Exhaustion of the polarization wave is then incomplete, and this leads to sustained multifrequency interactions and further bandwidth growth.

Although one might expect that any competing process would be well established for Z as large as 200, Z is in fact not an appropriate measure of gain for a parasitic wave. The point is that, whereas Z is defined in terms of the *input* pump intensity, what is needed is an *effective* gain–length Z^{eff} for the competing process that takes account of the fact that the pump intensity falls dramatically as a result of the dominant UMRG interactions. Our goal is thus to quantify this integrated gain–length, so that a realistic parametrization of any leakage of input energy into an unwanted line can be achieved.

For the general case of a competing process arising from a particular (ith) Raman transition, the steady-state conversion efficiency under conditions of constant pumping is determined by $Z_i = g_i I_0 z$, where g_i is the steady-state gain coefficient of the ith transition. We denote the *effective* gain–length in this case by Z_i^{eff}. To determine the relationship between Z and Z_i^{eff}, one needs to model the growth in the bandwidth $B(Z)$ of the multifrequency beam. Seeking a very simple model, we consider the linear approximation $B(Z) = 2(1 + \eta Z)$, where η controls the rate of bandwidth increase with Z. We also assume that the energy of the input beams is evenly distributed across the bandwidth, so that the intensity of the pump and Stokes beams can be written $I_{\text{p,S}}(Z) \approx 2I_0/B(Z)$. The logical gain–length parameter for the competing process is then

$$Z_i^{\text{eff}} = \int_0^z g_i I_{\text{p,S}}(z)\, \mathrm{d}z. \tag{12}$$

For a wave generated by the scattering of a pump beam from the ith Raman transition, it is straightforward to show that

$$Z_i^{\text{eff}} \approx \frac{g_i}{g}\frac{1}{\eta}\ln(1 + \eta Z). \tag{13}$$

Equation (13) assumes that there is an unlimited space–time region within which the parasitic wave can deplete the axial pump energy. However, as already noted, if the competing process is not collinear with the pump beam, a maximum value $Z_{\max}$ will apply. The simplest way to incorporate this feature in the model is to define an effective pump intensity (the one seen by the competing process) as $I_{\text{p,S}}^{\text{eff}}(Z) = f(Z)I_{\text{p,S}}(Z)$ where $f(Z) = 1$ for $Z \leqslant Z_{\max}$ and $f(Z) = 0$ for $Z > Z_{\max}$. One then finds that the maximum effective gain–length product is given by

$$Z_i^{\text{eff}} \approx \frac{g_i}{g}\frac{1}{\eta}\ln(1 + \eta Z_{\max}). \tag{14}$$

From the simulation data presented in figure 2, one can also use equation (12) to evaluate Z^{eff} directly. The results for the dispersionless case are presented in figure 3 (*a*), which displays three different forms for Z^{eff}, calculated using the pump intensity, the Stokes intensity and their average $[I_{\text{p}}(Z) + I_{\text{S}}(Z)]/2$. It can be seen that bandwidth generation leads to at least an order-of-magnitude reduction in the gain–length for competing processes. It is important to note that no curve gives $Z^{\text{eff}} > 25$, which implies that small seeds, arising from background noise or ASE, will not be amplified to any significant level. The large difference between Z^{eff} calculated using I_{p} and Z^{eff} calculated using I_{S} (curves 1 and 2 respectively) can be explained by the character of the solution shown in figure 2 (*a*). For $Z < 70$, the two estimates of Z^{eff} are relatively close, but thereafter the two curves diverge monotonically. This arises from the convergence of the solution to a fixed pattern

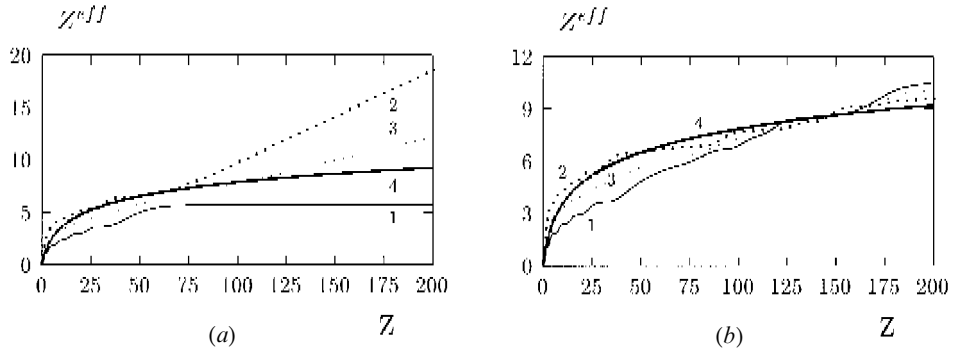

Figure 3. Effective gain–length Z^{eff} that would be experienced by a competing nonlinear process as a function of normalized distance Z for (*a*) $\gamma_1 = 0$, and (*b*) $\gamma_1 = 2.5 \times 10^{-3}$: curves 1 and 2, for Z^{eff} calculated directed from simulation data, using $I_{\text{p}}(Z)$ and $I_{\text{S}}(Z)$ respectively; curve 3, calculated using an average of the pump and Stokes intensities; curve 4, the simple analytical model of Z^{eff}.

in which $|A_0| \approx 0$ and $|A_{-1}| \approx 0.1$. To use the analytic expression for Z^{eff} (equation (13)) we set $g_i = g$ to maximize the gain available to the competing process and then choose $\eta = \frac{1}{2}$ to accommodate the linearized bandwidth and spectral intensity distribution approximations. The resultant curve, labelled 4 in figure 3 (*a*), proves to be a remarkably good measure of Z^{eff} as determined by the average of I_{p} and I_{S}.

Figure 3 (*b*) shows the corresponding results for $\gamma_1 = 2.5 \times 10^{-3}$. As in the dispersionless case, Z^{eff} derived from I_{p} is initially lower than Z^{eff} using I_{S}. This difference arises from a rapid energy transfer, from I_{p} to I_{S}, in the early stages of UMRG ($0 < Z < 3$). As indicated in figure 1, the UMRG process is largely independent of γ_1 for low values of Z. Thus, the curves for Z^{eff} also display this insensitivity. However, for higher Z, the complex evolution due to dispersion tends to average out the differences in Z^{eff} based on I_{p} and I_{S}. For the analytical model, we retain $\eta = \frac{1}{2}$ and find that, in this case, the agreement with Z^{eff} calculated using simulation data is quite spectacular. We also note that the more realistic calculations, which include dispersion, predict a much lower value of the net gain for a competing process. In this case, Z^{eff} ($Z = 200$) ≈ 10. Since, by definition, the main UMRG process exploits the Raman transition with highest gain coefficient, it can be seen from the g_i/g coefficient which appears in equation (13) that even this value of Z^{eff} may be an overestimate. We conclude that the relatively high efficiency of UMRG leads to the establishment of a sufficiently broad-band multifrequency beam that competing processes, which grow from background noise or ASE, remain below threshold ($Z^{\text{eff}} < Z^{\text{th}}$).

3.2. *Scattered light*

We now consider the potentially much more serious problems that could arise if a portion of an input beam is inadvertently scattered off-axis by the optical elements present and provides the seed for a competing process. This can be examined, in the context of system (8)–(11), by considering relatively large coherent off-axis seeds. It is possible that a 'winner-takes-all' situation might arise in the initial stages of UMRG in which either most of the energy remains on-

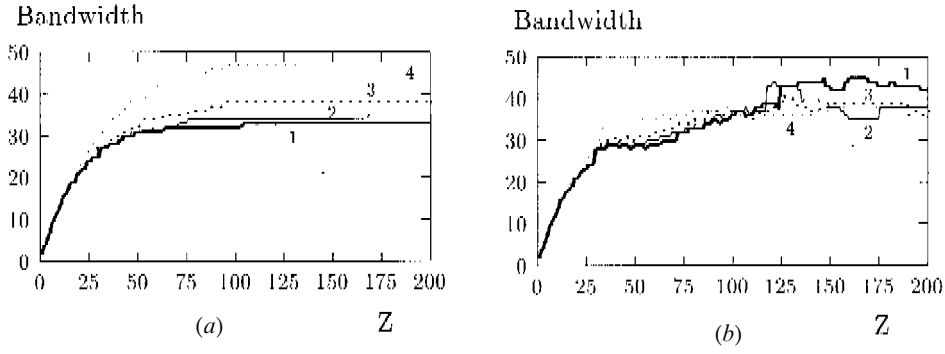

Figure 4. Bandwidth generated along the Raman cell when a competing process is initiated by part of a pump beam which is scattered off-axis for (*a*) $\gamma_1 = 0$ and (*b*) $\gamma_1 = 2.5 \times 10^{-3}$ (the curves are labelled according to the relative intensity of the scattered wave): curve 1, $|A'_{-1}(0)|^2 = 10^{-6}$; curve 2, $|A'_{-1}(0)|^2 = 10^{-3}$; curve 3, $|A'_{-1}(0)|^2 = 10^{-2}$; curve 4, $|A'_{-1}(0)|^2 = 10^{-1}$.

axis (as the multifrequency beam) or a strong off-axis seed depletes the pumps (draining sufficient energy off-axis to halt UMRG).

Simulations investigating a wide range of initial seed levels $|A'_{-1}(Z=0)|^2 = 10^{-13}$–$10^{-1}$ have been performed. However, it is sufficient to present results which deal only with relatively strong seeds. Bandwidth evolution for the dispersionless case is shown in figure 4(*a*). We obtain the quite remarkable result that the bandwidth of the multifrequency beam actually increases with the inclusion of a scattered wave. Indeed, for the largest seed level $|A'_{-1}(0)|^2 = 10^{-1}$, bandwidth enhancement is close to 50%. The presence of an off-axis wave upsets the convergence of the UMRG solution to a fixed pattern and prolonged interactions permit a much higher bandwidth to be attained before UMRG eventually saturates. After saturation, both the UMRG spectral profile and the intensity of the competing process are Z independent. We find that the competing process becomes appreciable, $|A'_{-1}(200)|^2 \approx 0.1$, when the scattered wave has an initial intensity of around 10^{-3}.

The results obtained when background dispersion is included are shown in figure 4(*b*). In this case, a similar bandwidth enhancement occurs in the earlier stages of UMRG, $Z < 70$, which roughly corresponds to the regime where the full impact of dispersion has not yet occurred. For larger propagation distances, the off-axis seed has a detrimental effect on bandwidth production. However, in all cases shown, the bandwidth generated at $Z = 200$ is still above the theoretical value for dispersionless UMRG ($B > B_0$). This detrimental effect can be attributed to the sustained amplification of the scattered wave which results from the replenishment of the pump wave due to the constantly evolving UMRG spectrum. For example, when the scattered wave is initiated with a relative intensity of 10^{-3}, the net effect of dispersion is to permit $|A'_{-1}(200)|^2 \approx 0.7$.

In figure 5 we present a summary of the dependence of bandwidth on the initial intensity of the competing process. These results confirm the trends suggested in the previous figures, showing bandwidth enhancement for $\gamma_1 = 0$ and, more importantly, that only a relatively small decrease in bandwidth occurs when dispersion is included. It is particularly surprising that the decrease is so small

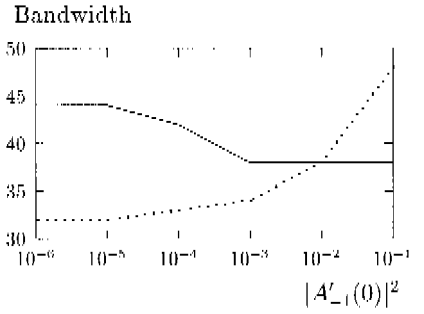

Figure 5. Dependence of the bandwidth at the output of the Raman cell on the initial intensity $|A'_{-1}(0)|^2$ of the competing process: (····), the dispersionless case; (——), data for $\gamma_1 = 2.5 \times 10^{-3}$.

when the initial intensity of the parasitic wave is 10% of the pump beam intensity. For the lower seed levels considered in figure 5, the output bandwidth appears to become insensitive to the initial intensity of the parasitic wave. Indeed, we can confirm that, for seed levels which are many orders of magnitude below those presented in figure 5, the output bandwidth remains at the level shown for $|A'_{-1}(0)|^2 = 10^{-6}$. This feature validates our approach to studying the role of spontaneous generation and ASE in the previous section and the conclusions reached there. For longer Raman cells ($Z > 200$), the $\gamma_1 = 0$ curve remains as shown in figure 5 since the UMRG spectral profile and the intensity of the competing process have become stationary with respect to Z. For $\gamma_1 = 2.5 \times 10^{-3}$, we find that higher Z leads to broadly the same conclusions, although some statistical (or chaotic) fluctuations appear owing to the complexity of the evolution of the waves.

4. Transient ultrabroad-band multifrequency Raman generation

Having investigated the generalized steady-state UMRG equations in detail, we now consider the transient effects that occur when the width of the input pulses is long, comparable or short when compared with the polarization dephasing time T_2 (approximately equal to 2.6 ns for H_2 gas at atmospheric pressure). In this section, we present results from the numerical solution of the full system (3)–(7). We consider Gaussian input pulses for the pump beams and the parasitic wave, although the precise choice of pulse shape has little or no effect on the conclusions. While, in steady-state modelling, one deals with the intensity of each wave, namely $|A_n|^2$, here the important parameters are the peak input intensity and the energy density $\int |A_n|^2 \, d\tau$. Accordingly, the bandwidth is defined in this section as the number of frequency channels containing comparable energy density.

We first consider the long-pulse regime, $t_p/T_2 = 10$, for which there should be reasonable correspondence with the steady-state limit. Figure 6 (*a*), for the dispersionless case, shows the role that the initial peak intensity of the competing process plays in determining the bandwidth generated along the Raman cell. The curves for $t_p/T_2 = 10$ are very close to the corresponding curves in figure 4 (*a*), which confirms the predictive power of the steady-state model. Figure 6 (*b*) shows the effect of dispersion; the corresponding data for CW beams is shown in figure 4 (*b*). It can be seen that, for relatively long input pulses, the overall trends are

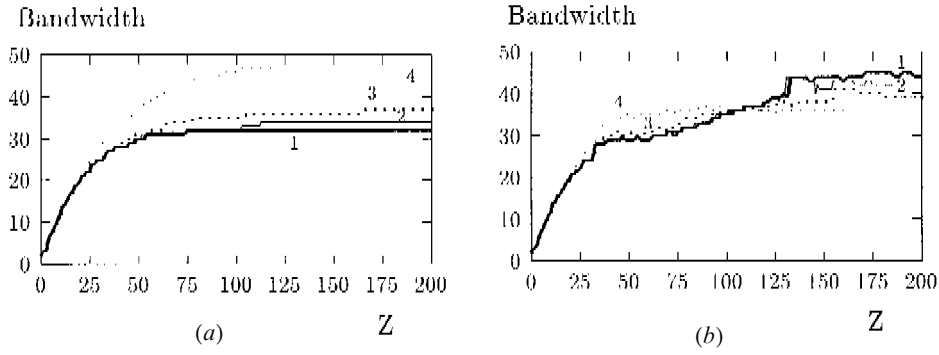

Figure 6. Growth in bandwidth of the multifrequency beam as a function of normalized distance Z for transient conditions $t_p/T_2 = 10$ (different curves correspond to different initial levels of the competing process, as defined in figure 4): (*a*) the $\gamma_1 = 0$ solutions; (*b*) the $\gamma_1 = 2.5 \times 10^{-3}$ solutions.

again accurately predicted by the much simpler CW model. In the initial stages, where dispersion plays a less significant role, bandwidth enhancement is evident. In the latter stages, replenishment of the pump wave leads to continued growth of the competing process and, eventually, this leads to a small reduction in bandwidth. The complexity of the evolution in dispersive UMRG leads to small quantitative differences between the CW and transient solutions in the latter stages.

Results for $t_p/T_2 = 1$, which lies between the quasi-CW and highly transient regimes, are shown in figure 7. Considering the dispersionless solutions (figure 7 (*a*)) we find the surprising result that there is a very strong insensitivity to seed level, even for relatively large scattered intensities. Each of the curves closely follows the UMRG solution in which the competing process is absent. Closer examination reveals that this insensitivity is associated with suppression of the amplification of the competing process. The overall features of bandwidth growth for $t_p/T_2 = 1$ and $\gamma_1 = 0$ are, firstly, a slower redistribution of the pump energy into the higher-order Stokes and anti-Stokes components and, secondly, a saturation of bandwidth growth at a higher level than that reached by the dispersionless CW solution. For dispersionless transient UMRG, the solution converges to a fixed pattern which involves a series of interlocking Raman soliton pulse trains in the time domain [4]. The results for $t_p/T_2 = 1$ when dispersion is included are shown in figure 7 (*b*). In addition to transiency suppressing the growth of the competing process, it can be seen that, to a large extent, this level of transiency also suppresses the effects of dispersion on bandwidth production for these propagation distances. Thus we find that the above conclusions, reached for the dispersionless case, are also true when dispersion is accounted for.

The bandwidth characteristics for the highly transient case of $t_p/T_2 = 0.1$ are shown in figure 8. Here, the sluggishness of the UMRG frequency conversion process is much more evident; the bandwidth generated at $Z = 200$ is only just over 20 waves of comparable energy. Once again, figures 8 (*a*) and (*b*) are for $\gamma_1 = 0$ and $\gamma_1 = 2.5 \times 10^{-3}$ respectively. In each case, transiency suppresses the growth of the competing process. It should be stressed that the $\gamma_1 = 0$ solution continues to grow in bandwidth if greater propagation distances are considered ($Z > 200$). A feature which arose in recent analytical work [14] was the prediction that the initial

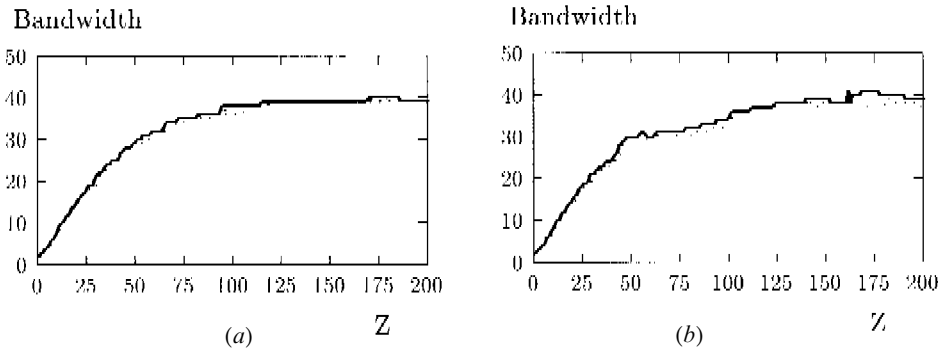

Figure 7. As figure 6, except that $t_p/T_2 = 1$.

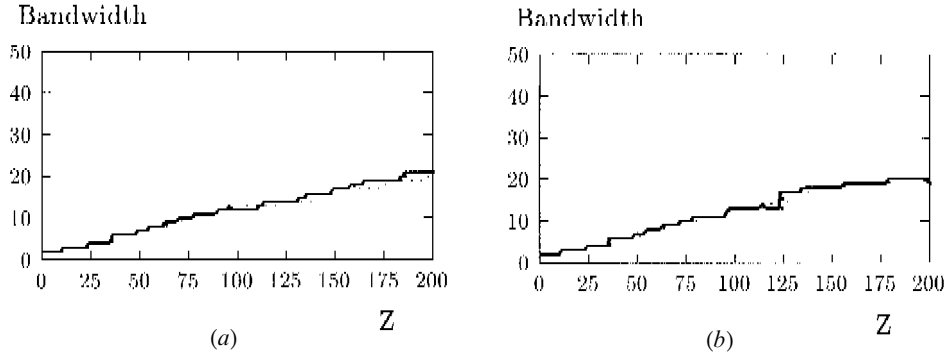

Figure 8. As figure 6, except that $t_p/T_2 = 0.1$.

stages of CW UMRG are essentially reproduced in the highly transient regime if one makes the transformation of $Z \rightarrow t_p Z/T_2$. Thus, comparing figure 6 (*a*), one sees that, for the quasi-CW case, $Z = 20$ results in the generation of a bandwidth of around 20 waves of comparable energy while, for $t_p/T_2 = 0.1$, one requires $Z \approx 200$ to attain the same bandwidth.

5. Conclusions

Recent experiments on UMRG in H_2 gas have produced output spectra that demonstrate competition between distinct Raman processes. We have undertaken a theoretical investigation to ascertain whether such additional parasitic processes necessarily accompany UMRG. We have derived a more general set of UMRG model equations and, for competing processes that arise from background noise or ASE, we have developed a simple analytical model that yields the effective gain–length Z^{eff} for a parasitic wave. Both full simulations and analytical results for a worst-case scenario predict that competing processes arising from these sources will remain below threshold. We have also studied the potentially more serious problems which could arise from a portion of an input beam which is scattered off axis by the optical elements present. The importance of the initial intensity of this off-axis wave has been assessed in conjunction with the roles played by transiency

and background dispersion. We have shown that the efficiency and character of UMRG, when driven by appropriately resonant and symmetric pumping, leads it to be robust against such effects. Our analytical model predicts a strong dependence of Z^{eff} on the steady-state gain coefficients involved. We expect that the use of high-pressure H_2 in experimental configurations has contributed to the appearance of parasitic vibrational components. Another important consideration is the dependence of the gain coefficients on the polarization of the pump beams. Thus experiments which have employed pump beams which are not linearly polarized may also be susceptible to the growth of competing processes.

Acknowledgments

We thank Dr M. J. Shaw for many useful discussions. This research was supported in part by UK Engineering and Physical Sciences Research Council grant No. GR/K 54748 and GR/L 90583 and INTAS grant No. 93-1103.

References

[1] Losev, L. L., and Lutsenko, A. P., 1993, *Kvantovaya Electron. (Moscow)*, **20,** 1054.
[2] McDonald, G. S., New, G. H. C., Losev, L. L., Lutsenko, A. P., and Shaw, M. J., 1994, *Optics Lett.*, **19,** 1400.
[3] McDonald, G. S., New, G. H. C., Losev, L. L., Lutsenko, A. P., and Shaw, M. J., 1995, Institute of Physics Conference Series No. 140 (Bristol: Institute of Physics), p. 85.
[4] McDonald, G. S., 1995, *Optics Lett.*, **20,** 822.
[5] McDonald, G. S., New, G. H. C., Losev, L. L., and Lutsenko, A. P., 1997, *J. Phys.* B, **30,** L719.
[6] Eimerl, D., Milam, D., and Yu, J., 1993, *Phys. Rev. Lett.*, **70,** 2738.
[7] Shen, Y. R., and Bloembergen, N., 1965, *Phys. Rev.*, **137,** A1787.
[8] Hermann, N., Norton, M., Twede, D., and Hackel, L., 1993, *Eleventh Conference on Lasers and Electro-Optics*, Baltimore, May 1993.
[9] Imasaka, T., Yamanishi, S., Kawasaki, S., and Ishibashi, N., 1993, *Appl. Optics*, **32,** 6633.
[10] Irie, Y., and Imasaka, T., 1995, *Optics Lett.*, **20,** 2072.
[11] Kawano, H., Lin, C.-H., and Imasaka, T., 1996, *Appl. Phys.* B, **63,** 121.
[12] Lin, C.-H., Ohnishi, T., and Imasaka, T., 1997, *Jap. J. appl. Phys.*, **36,** L412.
[13] Hickman, A. P., and Bischel, W. K., 1988, *Phys. Rev.* A, **37,** 2516.
[14] Losev, L. L., and Lutsenko, A. P., 1996, *Optics Commun.*, **132,** 489.